A Modified Gaussian Plume Model for Mobile *in situ* GHG Measurements: Supplemental Information

S1. Developing the asymmetric correction function

From the controlled release experiment, we noticed the severity of the asymmetric smoothing to the observed plumes caused by the LGR UGGA's lower flow rate and high mean residence time. The function we used to model the instrument response is an asymmetric function which is similar to a log-normal distribution. This function was chosen because the characteristic variables, σ and μ, move the function's vertical and horizontal components of the local maxima independently. We then determined a linear speed dependence for the hand fitted μ parameters which best matched observed concentration-distance plumes from the controlled release experiment with a simple linear regressions. Then, we determined a linear relation between the fitted σ and μ values. These speed dependent smoothing factors were then extrapolated to zero velocity, and then these parameter values ($\sigma = 0.517$, $\mu = 2.57$) were taken to the time ordinate parameters, or smooth
ing coefficients concentration-time inversion tests. Middling values between the fitted parameters, ($\sigma = 0.65$, $\mu = 2.2$) were used for the concentration-distance plumes. Both are shown in Figure S1. We normalize the function across a specified window length, which when convolved with an enhancement plume shape, results in an asymmetrically skewed curve with the same enhancement area as the original curve.

S1.1 Asymmetric smoothing and comparing quasi-coincidental plume transects.

During another mobile field campaign measuring plumes at the Petrolia landfill near Petrolia, Ontario, the LGR UGGA instrument was deployed in a rented vehicle as a mobile GHG labratory. The same Airmar WX220 was used as a GPS receiver in this setup. To compare quasi-coincidental observations, the UGGA equipped vehicle drove ~30m behind the ECCC Picarro vehicle through the same methane plume from transects recorded at 17:11 UTC on 2021-09-19[1]. We determined a temporal offset to align centre of each peak, and then convolved a the Picarro plume, interpolated to 1 second intervals, with the smoothing windows, and the results are shown in Figure S1. The r^2 coefficient for the observations increases from 0.29 for the Picarro observations and the UGGA , to 0.9 for the smoothed plume. This represents a significant improvement in the comparability of quasi-coincidental observations.

S2. Mobile Measurement Platforms

The bicycle based mobile laboratory consists of a Los Gatos Research (Mountain View, California, USA) Ultraportable Greenhouse Gas Analyzer (LGR UGGA), and an Airmar WX220 weather station. The inlet line was mounted at approximately 1.6m above ground, with the weather station slightly above, at a height of 1.8m. The LGR UGGA uses integrated cavity output spectroscopy to measure dry air mole fractions of methane, carbon dioxide, carbon monoxide and water vapour. The instrument has a stated precision of 3ppb, 0.4ppm, and 60ppm over a one second period for methane, carbon dioxide, and water vapour, respectively. Because of favourable riding conditions, a significant fraction of the data collected with this setup are in the summer months, from May until September of each year.

1 The data from that day's surveys can be viewed at: *https://www.atmosp.physics.utoronto.ca/GTA-Emissions/StaticMaps/2021-09-19/* .

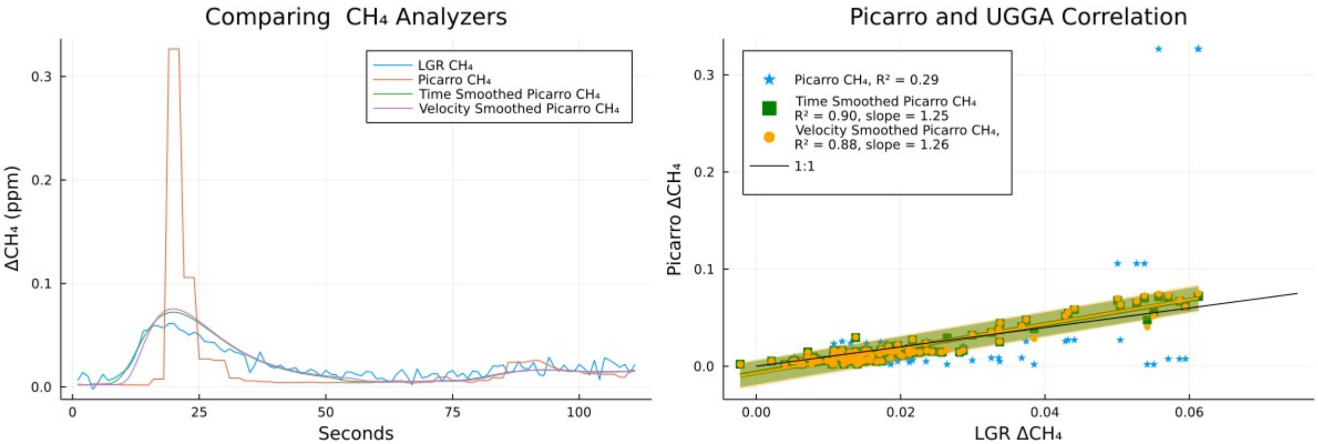

Figure S1: Left: Observed methane enhancement vs. time for quasi-coincidental Picarro and UGGA mobile observations. Right: the Picarro enhancement vs the UGGA enhancement. The unaltered Picarro plume is shown with blue stars, and the smoothed Picarro plumes are shown in green squares, and yellow circles for the time and velocity smoothing parameters respectively.

For the data considered in this study, Environment and Climate Change Canada's vehicle based laboratory has used both G1301 and G2401 cavity ring down spectrometers developed by Picarro (Santa Clara, California, USA) to measure mole fractions of methane, carbon dioxide, and water vapour. The G1301 analyzer had a precision of 1ppb, 0.2ppm, and 100ppm for CH_4, CO_2, and H_2O, over a 5 second integration period, respectively. The G2401 analyzer has a precision of <1ppb, <0.05ppm, and <30ppm for the same gasses over a 5s integration period. The inlet for the vehicle laboratory is roughly 2.5m above the ground.

S3. The Controlled Release Experiment

S3.1.Inversion Results by different stability class.

Figure S2: The location of the gas outlet from our controlled release experiment on 2021-10-20. Transects were driven on the road and bicycle path along Leslie street, directly downwind of the release location.

Table S1: Line of best fit parameters for the controlled release experiment Gaussian area inversions, with results plotted in Figure S3.

Inversion	Bike Unfiltered Slope	Bike Unfiltered Intercept	Bike Filtered Slope	Bike Filtered Intercept	Car Slope	Car Intercept	Combined Slope	Combined Intercept
Urban A/B	1.55 ± 0.66	7.3 ± 7.2	1.96 ± 0.80	0.3 ± 9.5	1.50 ± 0.71	1.3 ± 2.9	1.71 ± 0.34	0.8 ± 3.8
Urban C	1.01 ± 1.00	14.8 ± 11.1	1.66 ± 0.67	0.4 ± 7.9	1.18 ± 0.24	1.9 ± 2.5	1.39 ± 0.29	1.2 ± 3.2
Rural A	1.01 ± 1.01	14.8 ± 11.1	1.66 ± 0.67	0.4 ± 7.9	1.18 ± 0.24	1.9 ± 2.5	1.39 ± 0.29	1.2 ± 3.2
Rural B	1.25 ± 1.78	13.2 ± 19.6	1.19 ± 0.46	0.3 ± 5.5	0.83 ± 0.21	2.6 ± 2.2	0.98 ± 0.21	1.73 ± 2.4
Rural C	1.91 ± 0.54	-2.9 ± 6.0	1.14 ± 0.41	0.4 ± 5.0	0.75 ± 0.33	4.2 ± 3.5	0.90 ± 0.25	2.8 ± 2.8
σ_a Rural	0.87 ± 0.98	12.4 ± 10.8	1.18 ± 0.46	0.71 ± 5.5	0.83 ± 0.21	2.3 ± 2.3	0.98 ± 0.22	1.64 ± 2.4
σ_a Urban	1.50 ± 0.66	7.7 ± 7.2	1.94 ± 0.80	0.0 ± 9.5	1.20 ± 0.25	1.9 ± 2.7	1.52 ± 0.34	1.02 ± 3.84

The lines of best fit for the controlled release experiment inversions were calculated using the Julia language's LsqFit package. Based on the experimental conditions, in an unobstructed environment with low wind speeds and moderate insolation, the prescribed PSG stability class we used was Rural B. Further discussion of atmospheric stability classes is presented in SI section 6.

Plots of the estimated release rates for our recommended inversion strategies (smoothed plume area for the UGGA, and Gaussian plume area for the Picarro), for each stability class are shown in Figure S3, and parameters for the lines of best fit are presented in Table S1. Similar results for the enhancement height inversions are presented in Figure S4 and Table S2.

Table S2: Line of best fit parameters for the controlled release experiment Gaussian enhancement height inversions, with results plotted in Figure S4.

Inversion	Bike Gaussian Slope	Bike Gaussian Intercept	Bike Smoothed Slope	Bike Smoothed Intercept	Car Slope	Car Intercept
Urban A/B	0.41 ± 0.16	0.1 ± 1.9	2.03 ± 0.79	0.5 ± 9.4	1.43 ± 0.31	0.3 ± 3.3
Urban C	0.24 ± 0.09	0.1 ± 1.1	1.70 ± 0.65	0.4 ± 7.7	1.20 ± 0.24	-0.1 ± 2.7
Rural A	0.24 ± 0.09	0.1 ± 1.0	1.70 ± 0.65	0.4 ± 7.7	1.20 ± 0.24	-0.1 ± 2.7
Rural B	0.13 ± 0.04	0.1 ± 0.6	1.22 ± 0.44	0.3 ± 5.2	0.93 ± 0.23	0.1 ± 2.5
Rural C	0.09 ± 0.03	0.1 ± 0.4	1.16 ± 0.40	0.4 ± 4.6	0.43 ± 0.27	4.7 ± 2.9
σ_a Rural	0.12 ± 0.05	0.2 ± 0.6	1.20 ± 0.44	0.7 ± 5.2	0.65 ± 0.16	1.6 ± 1.8
σ_a Urban	0.41 ± 0.16	-0.1 ± 1.9	2.01 ± 0.79	0.1 ± 9.4	1.42 ± 0.29	-0.5 ± 3.1

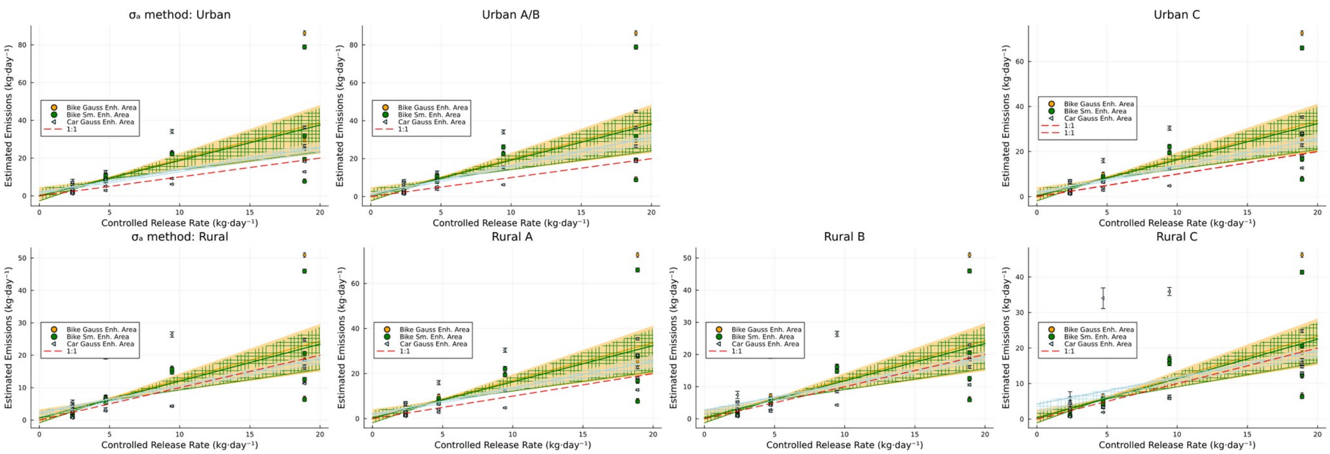

Figure S3: Controlled release experiment emissions estimates from the mobile labs using different stability classes. Smoothed area estimates shown in green with a vertical hatched ribbon, and the Gaussian area estimates for the bike are in orange with a solid ribbon, and the vehicle Gaussian area are estimates are shown in light blue with a diagonal hatched ribbon.

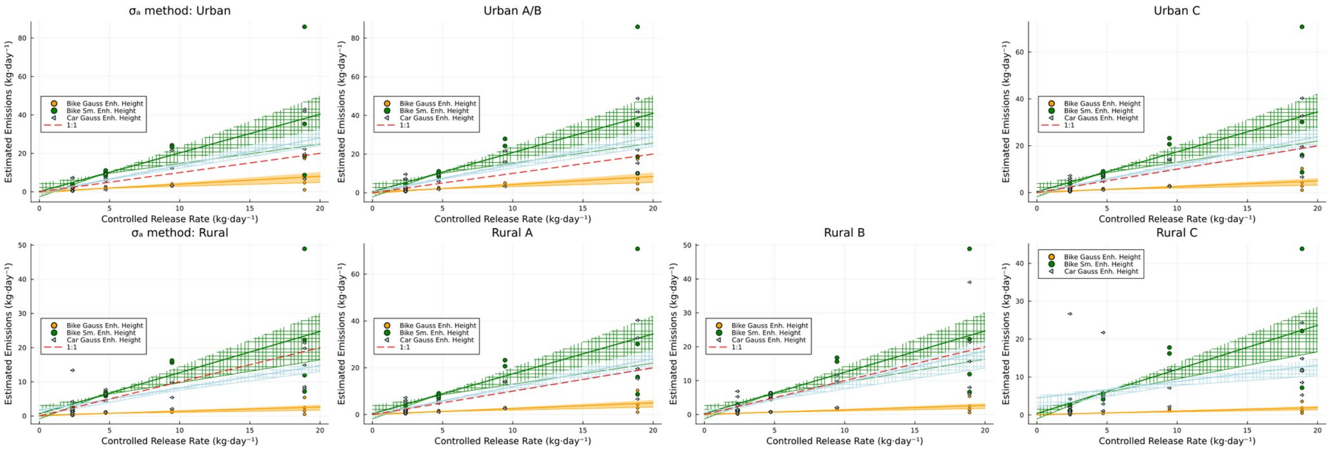

Figure S4: Controlled release experiment emissions estimates from the bike UGGA lab using different stability classes. Smoothed height estimates shown in green with a vertical hatched ribbon, and the Gaussian height estimates for the bike are in orange with a solid ribbon, and the vehicle Gaussian height are estimates are shown in light blue with a diagonal hatched ribbon.

S3.2 Controlled release analysis using the Weller 2019 algorithm

In addition to our Gaussian plume inversion methodology, we also evaluate the log-log statistical equation presented in Weller et al. 2019. This algorithm was originally designed to roughly estimate emissions rates from urban natural gas leaks for mobile surveys (which did not collect coincidental meteorological data), utilizing the Picarro G2301 GHG analyzers. This algorithm does not consider source location, atmospheric stability, or wind speed. Our controlled release experiment was designed to test the applicability of the Gaussian plume inversion technique for nearby sources, and was of a smaller scope than those used to calibrate the Weller algorithm. The estimates from the Weller et al. 2019 algorithm when applied to our controlled release data are presented in Figure S5.

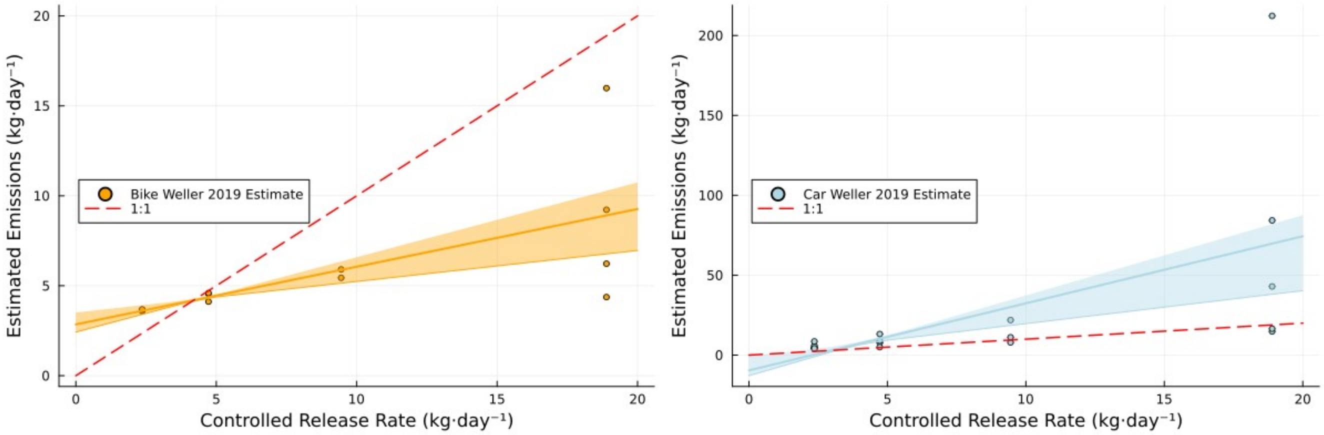

Figure S5: Methane emission estimates vs. known release rate calculated using the Weller 2019 statistical algorithm. Results from the bicycle UGGA laboratory are shown on the right, and the Picarro equipped vehicle on the left.

S3.3 Observed Winds During the Controlled Release Experiment

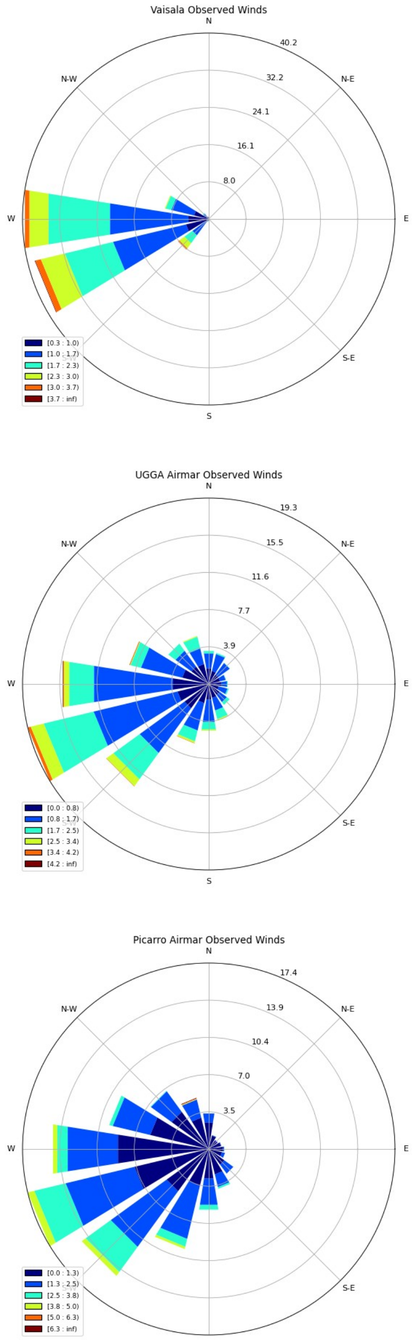

Figure S6: Wind roses for the stationary Vaisala (top), and mobile Airmar weather sensors on the bicycle UGGA lab (middle) and ECCC Picarro vehicle (bottom).

S3.4 Filtering Inversions by Minimum Transect Distance

During our controlled release experiment on 2021-10-20, the minimum downwind transect distances recorded by each platform are shown in Figure S7. Transects completed by bicycle were constrained to the inner shoulder of the road, the adjacent sidewalk, and bicycle paths. After we noticed a high bias in the estimates from the nearest bicycle transects, we filtered out all of the bicycle transects which were less than 6.2m from the source.

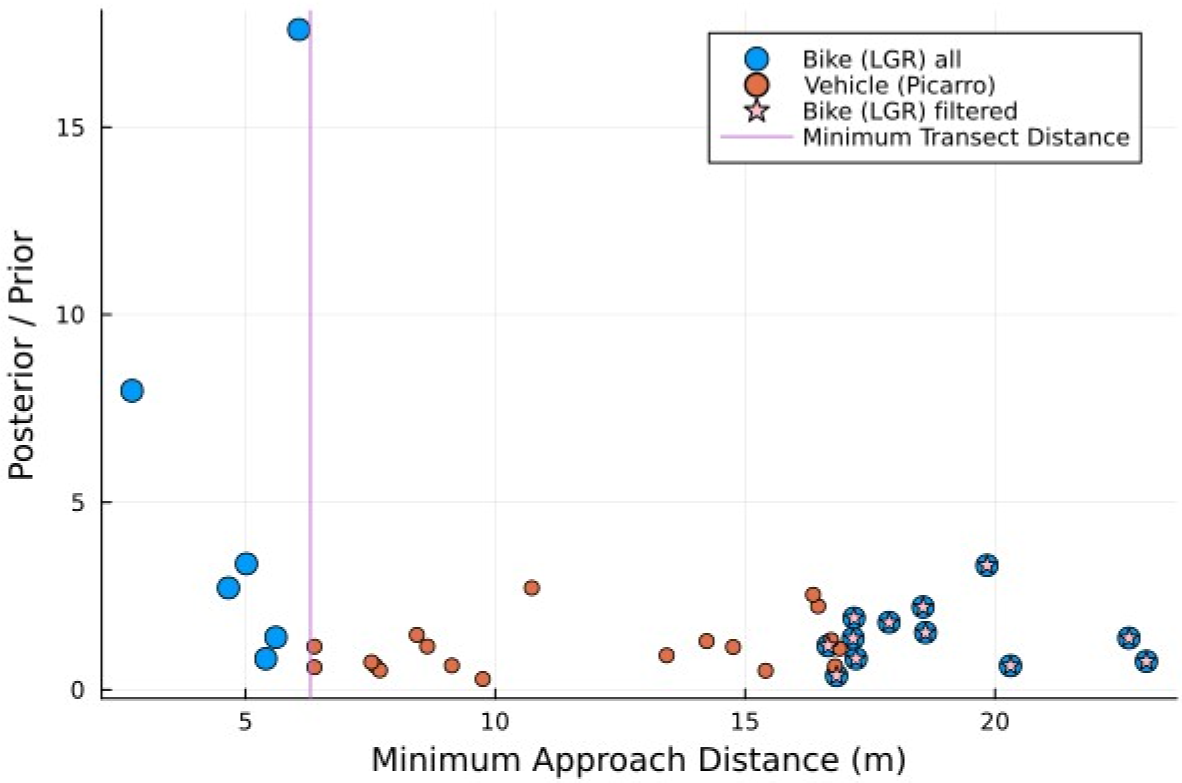

Figure S7: Ratio of estimated and controlled release rate versus transect minimum approach distance.

S3.5 Inversion sensitivity to other model parameters

The emissions estimated from Gaussian plume inversions are dependent on initial model parameters, such as the wind speed, direction, location of the source and observations. We assume that the source location and GPS measurement coordinates are accurate.

In order to investigate our primary inversion strategy's sensitivity to the wind speed and direction, we performed a perturbation analysis. For wind direction, we recalculated the distance-concentration area inversions by rotating the wind 0.5 standard deviations of the measured wind vectors from the transect duration. Overall, these had little impact on the estimated emissions rates. For the wind speeds tests, we multiplied measured wind speeds by 2/3 and 4/3, to demonstrate the linear dependence of our inversion scheme to wind speed.

S3.5.1 Wind Direction

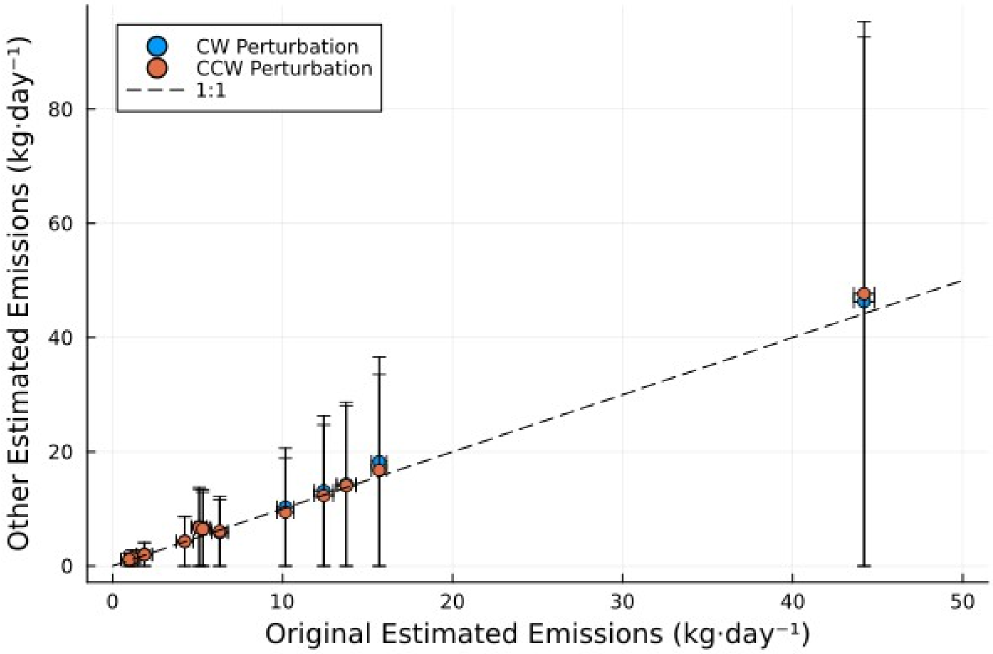

Figure S8: 2021-10-20 bike controlled release results using stability Urban C with +/- 0.5 standard deviations of measured wind direction. CW data are inversion results with the wind vector rotated in a clockwise directions, while CCW indicates a counterclockwise perturbation.

S3.5.2 Wind Speed

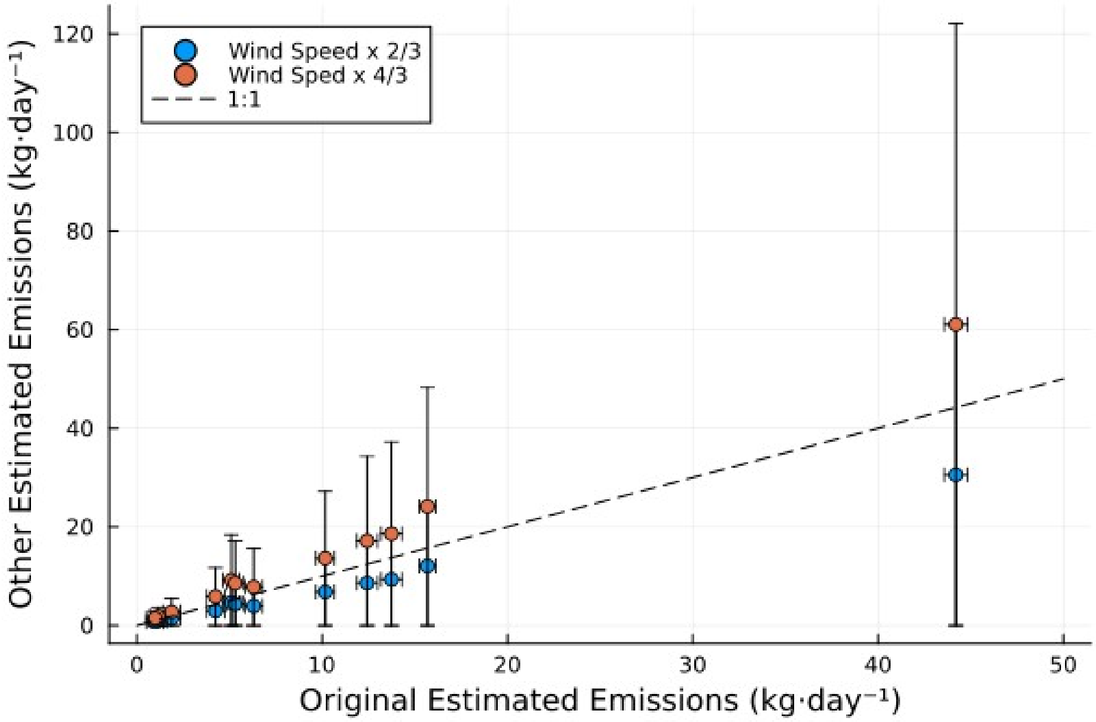

Figure S9: 2021-10-20 bike controlled release results with stability Urban C, reevaluated using 2/3 and 4/3 of measured wind speed.

S4. Ashbridge's Bay Inversions

S4.1 The FLAME-GTA inventory estimate

The formula from the FLAME-GTA inventory, for facilities with gas capture and destruction, is as follows,

$$F_{CH_4} = V_{gas} \times f_{CH_4} \times \rho_{CH_4} \times (1/C_{eff} - D_{eff}) \quad ,$$

where F_{CH_4} is the methane emission in metric tons of methane per year, V_{gas} is the volume of biogas produced, f_{CH_4} is the fraction of methane in the biogas by volume, ρ_{CH_4} is the density of methane gas at standard atmospheric conditions (0.000674 t/m^3), C_{eff} is the biogas collection efficiency (assumed 0.98 for enclosed vessels), and D_{eff} is the biogas destruction efficiency (between 0.95 and 0.98 depending on the destruction device) .

S4.2 Inversion Results by Temporal Period

In the following subsubsections, we present our estimates of ABWWTP emissions by year, for the four years considered in this work.

S4.2.1 Inversion Results by Year

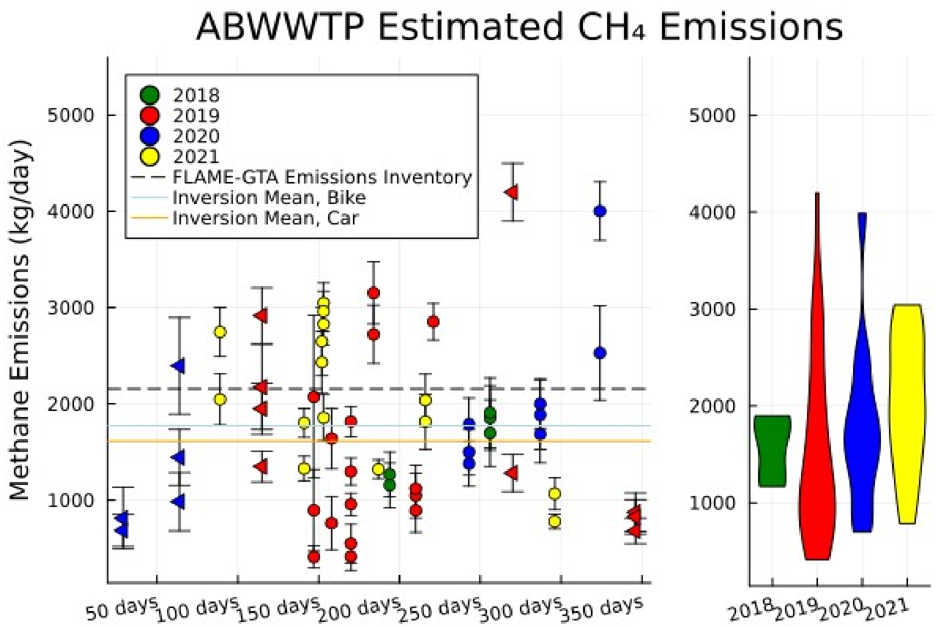

Figure S10: Left: Inversion results for all transects of ABWWTP. Bike data are shown with circle markers, and car data are triangles. Right: Violin plots showing the relative distribution frequency of different estimated emissions rates from each year's observations.

S.4.2.2 Inversion Results by Month

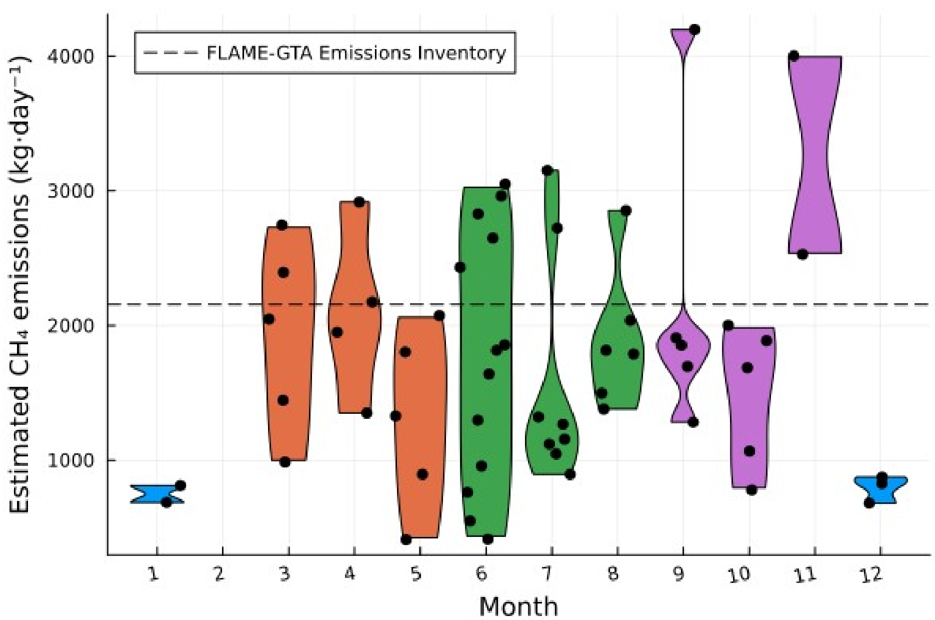

Figure S11: Violin and dot plots showing the relative distribution frequency of different estimated emissions rates from each months' observations at ABWWTP. The horizontal position of the dots within the violin plots is random.

S4.3 Results using Various Model Parameters Perturbations.

The Gaussian plume inversion strategy is dependent on model parameters, such as stability class and wind speed and direction. In this subsection, we present how our ensemble of inversions would change if initial model parameters were changed. We show the impact of stability class choice, wind direction, and wind speed perturbations. For the wind direction perturbation test, we reprocess inversions with by adding or subtracting 0.5 times the standard deviation of the measured wind direction. For the wind speed perturbations, we reprocess inversions using 0.7 and 1.3 times the measured average windspeeds.

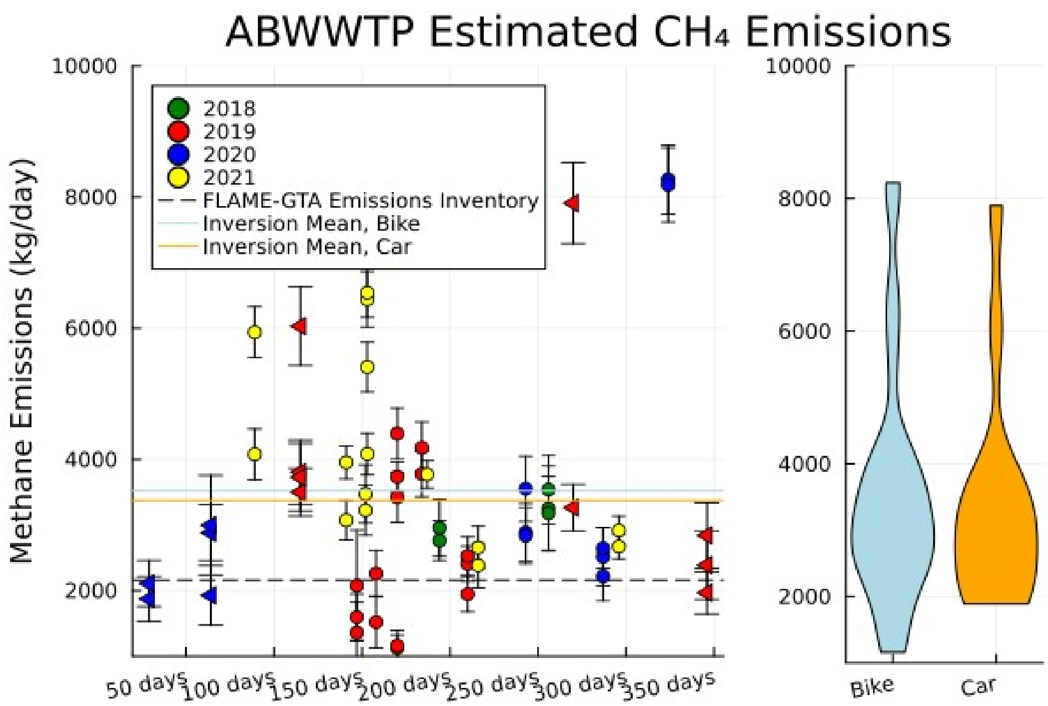

Figure S12: Left: Inversion results for all transects of ABWWTP using the Brigg's urban stability classes instead of the rural stability classes. Bike data are shown with circle markers, and car data are triangles. Right: Violin plots showing the relative distribution frequency of different estimated emissions rates from each platforms' observations.

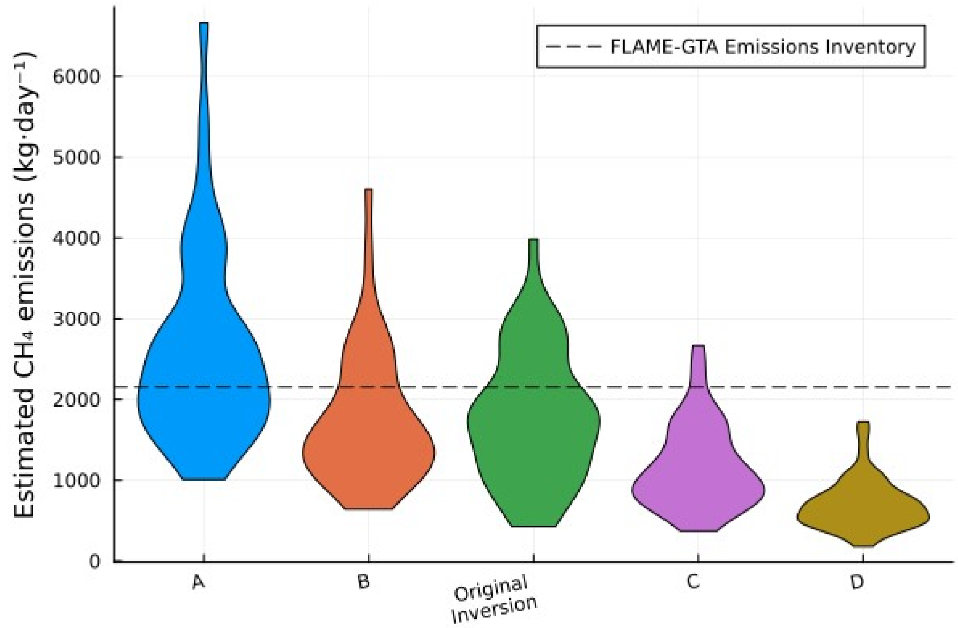

Figure S13: Violin plots showing the relative distribution frequency of emissions rates using specific rural stability classes for our ABWWTP inversions. The violin plot of the original inversions is shown in the centre in green.

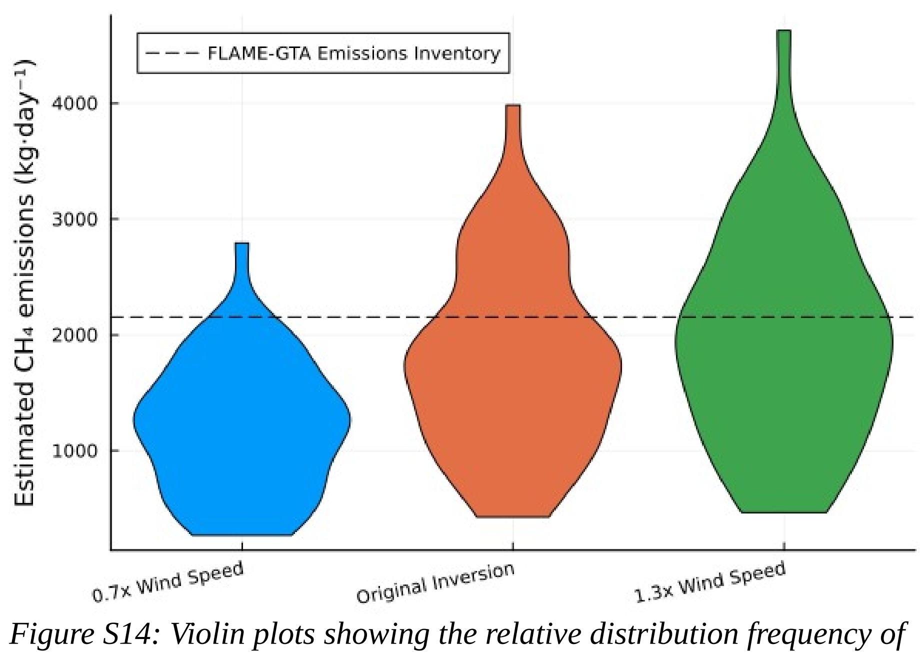

Figure S14: Violin plots showing the relative distribution frequency of emissions rates estimated from inversions with a multiplicative perturbation to the measured average windspeed as measured by the Airmar WX220s for our ABWWTP inversions. The violin plot of the original inversions is shown in the centre in dark orange.

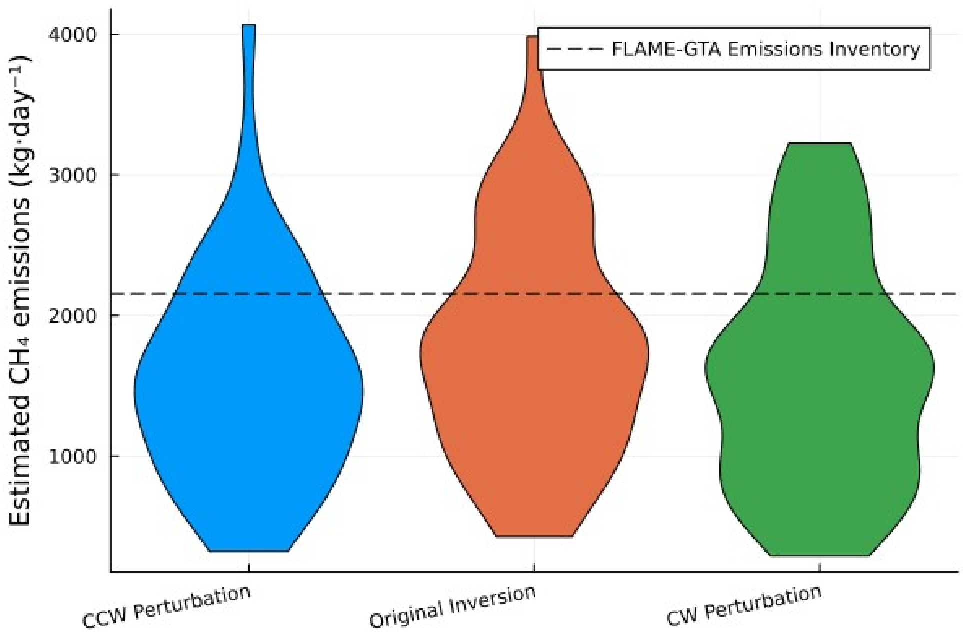

Figure S15: Violin plots showing the relative distribution frequency of emissions rates estimated from inversions with a multiplicative perturbation to the measured wind direction variability as measured by the Airmar WX220s for our ABWWTP inversions. The violin plot of the original inversions is shown in the centre in dark orange.

S4.4. ABWWTP Inversion Parameters

Table S3: Transect numbers and inversion parameters for ABWWTP Vehicle Transects

Date_Transect #	**Stability Class**	**Number of Integration Slices**	**Posterior Emissions (kg/day)**	**Posterior Error (kg/day)**	**Data Filename**
2019-04-25_1	C	2	1349.8765978935	161.231479961511	sync_data_2019-04-25_Truck
2019-04-25_2	C	3	2916.84909577519	289.040591885205	sync_data_2019-04-25_Truck
2019-04-25_3	B	3	1949.8216088839	266.677824072728	sync_data_2019-04-25_Truck
2019-04-25_4	C	2	2174.55177997144	440.107044265125	sync_data_2019-04-25_Truck
2019-09-27_1	D	2	4197.51523057618	300.339608749208	sync_data_2019-09-27_Truck
2019-09-27_2	D	3	1281.79027522266	192.682927380736	sync_data_2019-09-27_Truck
2019-12-12_1	D	2	680.741667875412	131.193844110173	sync_data_2019-12-12_Truck
2019-12-12_2	D	2	874.492768552581	201.764877615494	sync_data_2019-12-12_Truck
2019-12-12_3	D	3	826.978294178305	178.588918687398	sync_data_2019-12-12_Truck
2020-01-30_1	D	3	812.620683234938	320.436314262498	sync_data_2020-01-30_Truck
2020-01-30_2	D	2	685.753404035207	165.857306136528	sync_data_2020-01-30_Truck
2020-03-05_1	B	2	1444.18357390014	290.827067500607	sync_data_2020-03-05_Truck
2020-03-05_2	B	2	2394.89127927294	501.856224194356	sync_data_2020-03-05_Truck
2020-03-05_3	B	2	985.115515438051	302.844144717308	sync_data_2020-03-05_Truck

Table S4: Transect information and inversion parameters for ABWWTP Bicycle Transects

Date_Transect #	Stability Class	Number of Integration Slices	Posterior Emissions (kg/day)	Posterior Error (kg/day)	Data Filename
2018-07-13_1	C	3	1155.54084370193	233.12280545222	sync_data_2018-07-13
2018-07-13_2	B	2	1267.09793850399	234.16683291535	sync_data_2018-07-13
2018-09-13_1	B	3	1853.57190082979	334.280422183308	sync_data_2018-09-13
2018-09-13_2	B	3	1907.3310354796	363.606396485316	sync_data_2018-09-13
2018-09-13_3	B	3	1695.78944612676	345.28485734021	sync_data_2018-09-13
2019-05-27_1	D	3	410.662694785916	115.113390638513	sync_data_2019-05-27
2019-05-27_2	D	3	894.569419422288	423.826602110733	sync_data_2019-05-27
2019-05-27_3	D	2	2073.6	844.660352094261	sync_data_2019-05-27
2019-06-07_1	A	2	1640.20733115615	314.747607243143	sync_data_2019-06-07
2019-06-07_2	B	3	760.688559140317	277.402861872351	sync_data_2019-06-07
2019-06-19_1	D	2	413.741014207417	145.228734867078	sync_data_2019-06-19
2019-06-19_2	C	2	548.653528393215	202.448707263482	sync_data_2019-06-19
2019-06-19_3	D	2	1296.51203985171	139.290706048227	sync_data_2019-06-19
2019-06-19_4	C	2	1814.82371738185	156.324529293532	sync_data_2019-06-19
2019-06-19_5	D	2	957.197813463807	115.986814916365	sync_data_2019-06-19
2019-07-03_1	A	3	2721.74487855647	301.387633235863	sync_data_2019-07-03
2019-07-03_2	A	3	3151.8839577495	322.289645824223	sync_data_2019-07-03
2019-07-29_1	C	2	894.259647924485	229.345242189047	sync_data_2019-07-29
2019-07-29_2	C	2	1047.41486324639	234.821084677238	sync_data_2019-07-29
2019-07-29_3	C	2	1119.44564931656	242.319553604087	sync_data_2019-07-29
2019-08-09_1	B	3	2853.37044243056	189.271628316093	sync_data_2019-08-09
2020-08-31_1	B	3	1378.63229685807	233.739727681135	sync_data_2020-08-31
2020-08-31_2	B	3	1788.27167431377	271.337446708376	sync_data_2020-08-31
2020-08-31_3	B	4	1497.47399097418	236.867073903044	sync_data_2020-08-31
2020-10-14_1	A	5	1686.06041608361	296.565630551795	sync_data_2020-10-14
2020-10-14_2	A	3	1886.19030647249	358.774175265981	sync_data_2020-10-14
2020-10-14_3	A	3	2000.86769266902	257.743903732469	sync_data_2020-10-14
2020-11-20_1	B	3	4001.73514024337	303.505781965257	sync_data_2020-11-20
2020-11-20_2	C	3	2528.14435125656	488.799393571149	sync_data_2020-11-20
2021-03-30_1	B	3	2046.4518133174	265.140145377635	sync_data_2021-03-30
2021-03-30_2	B	3	2745.61501743398	255.177015163751	sync_data_2021-03-30
2021-05-21_1	B	4	1802.63574686914	150.878707609937	sync_data_2021-05-21
2021-05-21_2	B	4	1328.91507761172	127.512181650766	sync_data_2021-05-21
2021-06-01_1	A	4	2647.88241254091	355.121858976514	sync_data_2021-06-01
2021-06-01_2	A	4	2431.17755238121	320.873490173098	sync_data_2021-06-01
2021-06-02_1	B	4	3049.16486253711	207.514870195597	sync_data_2021-06-01
2021-06-02_2	B	3	2961.0128500933	208.820270939852	sync_data_2021-06-01
2021-06-02_3	B	3	2828.07652257634	218.168851065685	sync_data_2021-06-01
2021-06-02_4	B	3	1856.35973421698	239.703680836213	sync_data_2021-06-01
2021-07-06_1	C	3	1320.87630836742	98.8462992853891	sync_data_2021-07-06
2021-08-04_1	A	3	2036.8624207932	271.498948956524	sync_data_2021-08-04
2021-08-04_2	A	3	1814.73220963208	286.000892445155	sync_data_2021-08-04
2021-10-23_1	D	3	778.690842522201	77.5548459329506	sync_data_2021-10-23
2021-10-23_2	C	3	1066.3286952923	166.244940846277	sync_data_2021-10-23

S5. Instrument Calibration

For our analyzers used in mobile *in situ* surveys, we use the raw dry air mole fractions of methane recorded on each of the GHG analyzers. We conduct irregular calibration experiments using ambient concentration dry air tanks which have been measured by reference CRDS spectrometers, which are regularly calibrated and traceable to the WMO standard scale. Typically, our instruments show a good linear correlation near the ambient concentration range for urban methane observations (1.95-2.2 ppm). No long term drifts have been observed with the LGR UGGA. Between the 2018 and 2019 summer measurement campaigns, the LGR UGGA was returned to the manufacturer for maintenance, and calibration offsets significantly improved from ~80ppb to <15ppb.

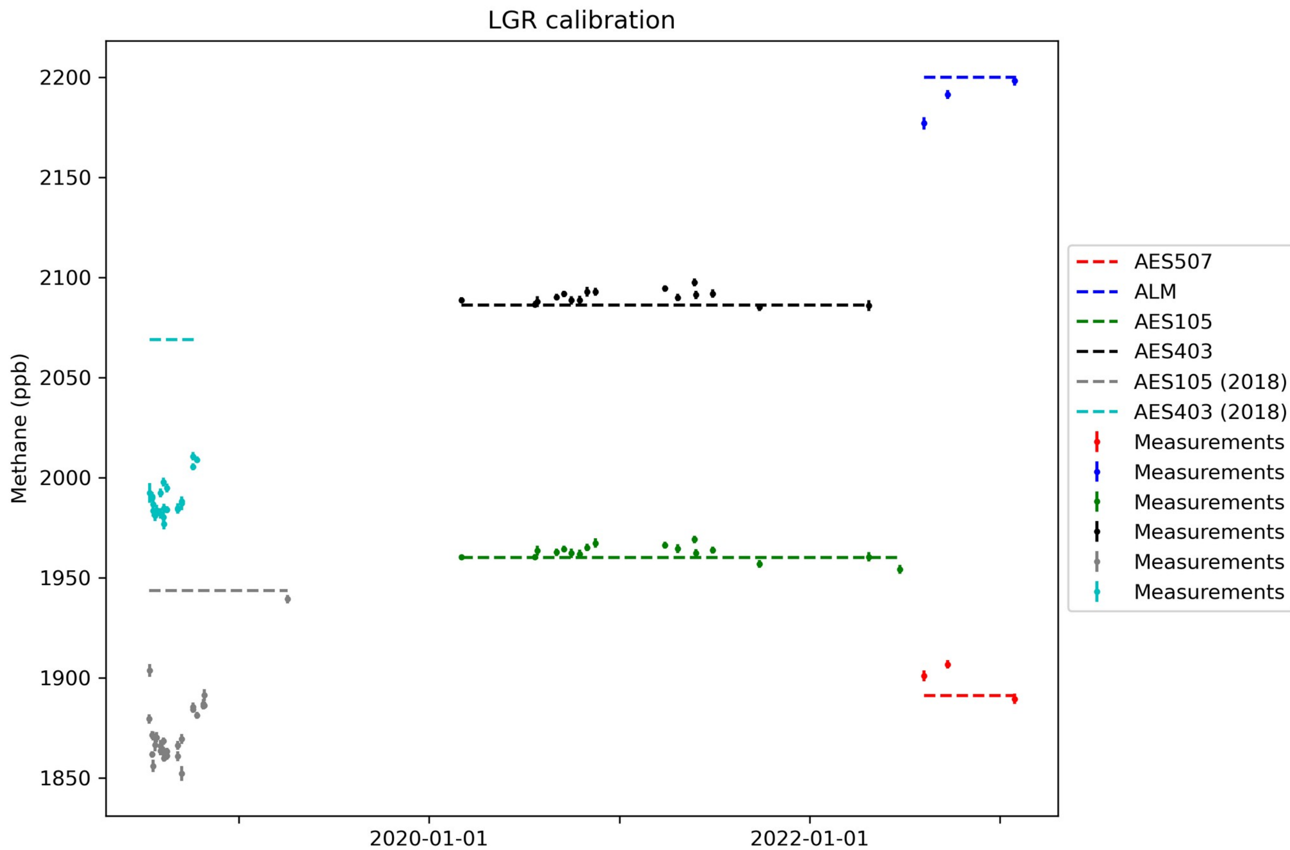

Figure S16: Record of calibration experiments conducted with the LGR UGGA. The improvement in instrument calibration between 2018 and 2019 occurred after the instrument had been returned to the manufacturer for maintenance.

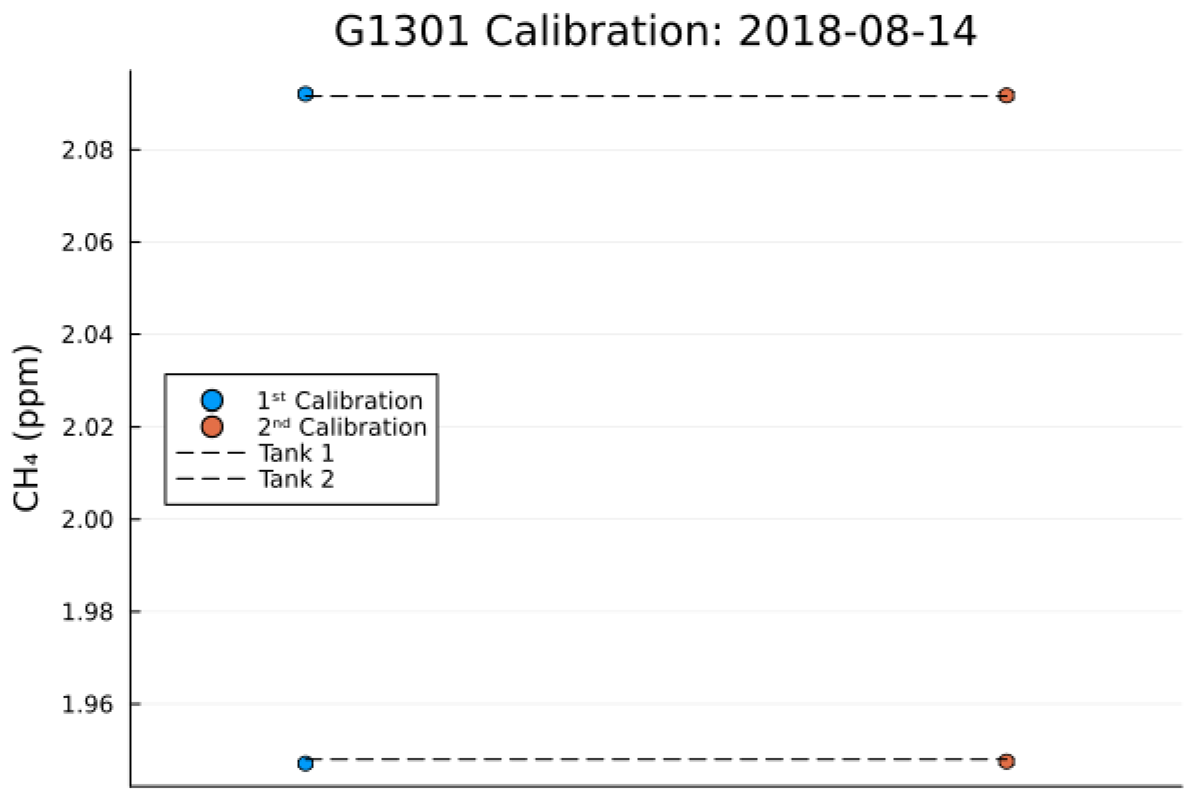

Figure S17: Results from the calibration experiment performed on the Picarro G1301 instrument used for the vehicle based lab surveys from August 2018 to September 2019.

Recently, we have began to investigate the analyzer's performance over a span of methane concentration ranges (2-8 ppm). We noticed a potential non-linearity of the LGR UGGA with respect to the concentrations measured by the Picarro G2401 in concentrations greater than 5ppm. We do not account for this potential non-linearity in this paper, as none of the measured methane concentrations in the analyzed plumes are in excess of 3.5 ppm.

S6. Controlled Release Stability Classes

Gaussian plume stability class represents the largest source of uncertainty for our emissions estimates. For the controlled release experiment, we had stationary in situ meteorology measurements, which allowed us to estimate transect-specific stability classes using the σ_a version of the modified sigma theta method for determining stability classes, as presented in U.S. EPA's Meteorological Monitoring Guidance for Regulatory Modeling Applications[1].

Release Rate (kg/day)	Transect (Bike)	σ_a stability class
2.3	2	A
2.3	3	B

2.3	4	C
4.7	1	B
4.7	2	B
4.7	3	A
9.4	2	B
9.4	3	C
18.9	1	B
18.9	2	B
18.9	3	C
18.9	5	B
	Transect (Car)	
2.3	1	D
2.3	2	C
2.3	3	A
2.3	4	D
2.3	5	D
2.3	6	C
2.3	7	C
4.7	1	A
4.7	2	B
4.7	3	B
4.7	4	C
9.4	1	B
9.4	2	B
9.4	3	D
18.9	1	D
18.9	2	B
18.9	3	C
18.9	4	B
18.9	5	C

(1) Bailey, D.; Brode, R.; Bennett, E.; Dicke, J.; Eskridge, R.; Garrison, M.; Irwin, J.; Koerber, M.; Lockhart, T.; Method, T.; Perkins, S.; Wilson, R.; Cannady, B. *Meteorological Monitoring Guidance for Regulatory Modeling Applications*; EPA-454/R-99-005; US EPA: Research Triangle Park, 2000; p 170. https://www.epa.gov/sites/default/files/2020-10/documents/mmgrma_0.pdf (accessed 2023-07-27).